sustainability

MDPI

Article

Integrated Machine Learning Framework-Based Optimization of Performance and Emissions of Nanomaterial—Integrated Biofuel Engine

Sooraj Mohan [1], K. Ashwini [2], Ranjan Kumar Ghadai [1], Akash Nag [3], Jana Petrů [3] and P. Dinesha [1,*]

[1] Department of Mechanical and Industrial Engineering, Manipal Institute of Technology, Manipal Academy of Higher Education, Manipal 576104, India
[2] Department of Artificial Intelligence and Machine Learning, Shri Madhwa Vadiraja Institute of Technology and Management, Bantakal, Udupi 574115, India
[3] Faculty of Mechanical Engineering, VŠB—Technical University of Ostrava, 70800 Ostrava, Czech Republic
* Correspondence: dinesha.p@manipal.edu

Abstract

This study examines the effects of injection timing and cerium oxide (CeO_2) nanoparticle (NP) size on NOx emissions and brake thermal efficiency (BTE) in a compression ignition engine, contributing to Sustainable Development Goals 7 and 13. Experiments were conducted at four load conditions (25–100%) using NP sizes of 10 nm, 30 nm, and 80 nm. An artificial neural network integrated with multi-objective particle swarm optimization (ANN-PSO) was employed to identify optimal operating parameters. The optimized configurations improved BTE and reduced NOx emissions across all loads; for example, at 75% load, BTE increased from 30.38% (average) to 32.13% (optimum), while simultaneously reducing the NOx emissions from 1322 ppm (average) to 1272 ppm (optimum). Analysis of variance (ANOVA) confirmed load as the most significant factor ($p < 0.001$), followed by injection timing and NP size. The model predictions closely matched experimental results, validating the optimization approach. The optimization suggests an interpolated optimal NP size of approximately 45 nm, highlighting the potential for further exploration. This integrated experimental and computational approach offers a promising framework for improving combustion efficiency and reducing emissions, thereby advancing cleaner and more sustainable fuel technologies.

Keywords: clean combustion; energy efficiency; NOx emission; sustainable fuel technologies; optimization

Academic Editor: Alessandro Franco

Received: 26 August 2025
Revised: 5 October 2025
Accepted: 8 October 2025
Published: 11 October 2025

Citation: Mohan, S.; Ashwini, K.; Ghadai, R.K.; Nag, A.; Petrů, J.; Dinesha, P. Integrated Machine Learning Framework-Based Optimization of Performance and Emissions of Nanomaterial—Integrated Biofuel Engine. *Sustainability* **2025**, *17*, 9004. https://doi.org/10.3390/su17209004

1. Introduction

The combustion of fossil fuels in the industrial and transport sectors intensifies global warming and air pollution [1], with 2024 CO_2 emissions reaching a record 37.8 Gt [2]. To meet UN Sustainable Development Goals 7 and 13 [3], research focuses on cleaner combustion and renewable fuels [4]. Fuel injection pressure and timing critically influence atomization [5–8], combustion duration, and emission formation. Biodiesel, oxygenated additives [9–14], and metallic nanoparticles have demonstrated improved brake thermal efficiency and reduced CO, HC, and smoke emissions [15–19]. Cerium oxide nanoparticles, in particular, enhance combustion and thermal conductivity [20], resulting in lower fuel consumption and optimized emission characteristics at appropriate particle sizes and concentrations.

The literature review indicates extensive studies on nanoparticle–biodiesel blends examining engine performance and emissions. However, limited research has explored the influence of nanomaterial size in B20 blends under varying injection timings. As fuel injection timing critically governs ignition delay and combustion quality, this study investigates the combined effect of nanoparticle size and injection timing on the performance and emissions of a biodiesel-fueled engine. Unlike prior studies, the present research jointly optimizes these parameters using a machine learning-assisted, load-specific optimization framework validated across multiple operating conditions.

2. Methods

2.1. Experimental

Waste cooking oil biodiesel was procured from a local biodiesel development center. The B20 biodiesel blend was produced by mixing 20% (by volume) of neat biodiesel with 80% (by volume) mineral diesel. The physicochemical properties of the fuel blend were determined as per ASTM and tabulated in Table 1. Cerium oxide nanoparticles (NP) of 10, 30, and 80 nm sizes were purchased from the vendor. Three different fuel blends were prepared using 10, 30, and 80 nm size nanoparticles at a constant concentration of 80 ppm. The prepared fuel blends were represented as B20-10, B20-30, and B20-80. The surfactant, dodecenylsuccinic anhydride (DDSA-$C_{16}H_{28}O_3$), was used to confirm better dispersion of cerium nanoparticles in the biodiesel blend. Ultra-sonification was carried out for 0.5 h to ensure a good distribution of ceria nanoparticles in the fuel blends.

Table 1. The physicochemical properties of the fuel blend.

Property	Diesel	WCO Neat Biodiesel	B20 Biodiesel
Density (kg/m^3)	825	880	843
Lower calorific value (MJ/kg)	43.2	39.6	40.3
Kinematic viscosity (mm^2/s)	3.85	5.3	3.7
Flash point (°C)	55	135	66

The test setup consists of a four-stroke single-cylinder CI engine with an eddy current dynamometer for loading the engine. The test setup specifications are given in Table 2. The schematic of the setup is depicted in Figure 1. Engine cooling is achieved by circulating water through the engine cooling jacket. A burette was used to measure the fuel flow, and the time taken to consume 20 cc was measured. The experiments were conducted at three different fuel injection timings: 24° bTDC retarding, 30° bTDC advancing, and the standard fuel injection timing of 27° bTDC. The prepared fuel and nanoparticles combinations were tested at these engine operating conditions. This data was used to calculate the brake thermal efficiency (BTE) of the engine. The concentration of exhaust emissions was measured using an AVL exhaust gas analyzer. The experiments were conducted in three replicates and the average of the three has been reported in this study.

Table 2. Specifications of diesel engine.

Type	Single Cylinder, Four Stroke, Air Cooled Engine
Make	Kirloskar
Bore × stroke	87.5 mm × 110 mm
Compression ratio	17.5:1
Rated output	5.2 kW at 1500 rpm
Injection pressure	240 bar
Swept volume	661 cm^3

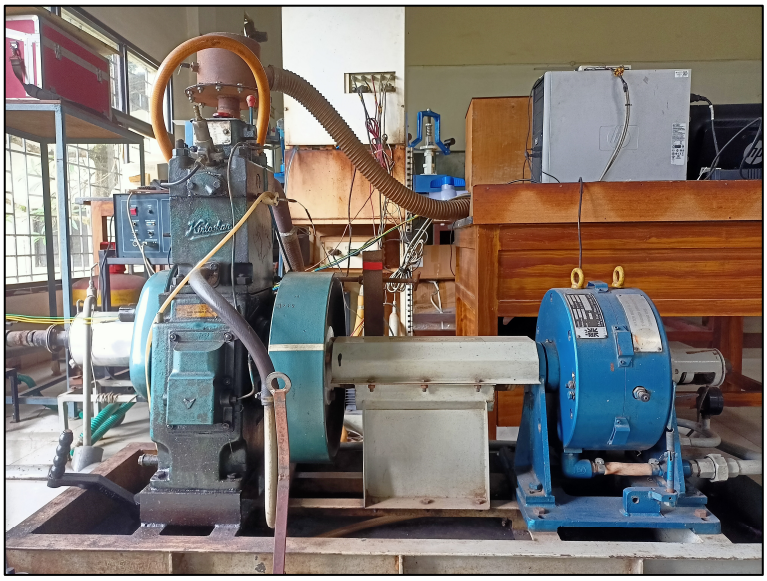

(**a**)

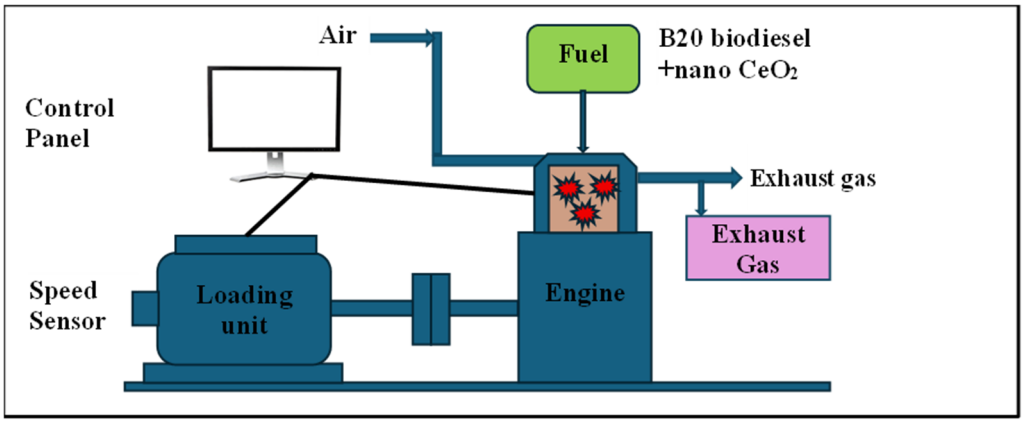

(**b**)

Figure 1. (**a**) Actual engine setup used in the study. (**b**) Representative diagram of the engine test setup.

2.2. Analysis of Variance (ANOVA) Testing

To statistically assess the influence of input parameters (IT, Load, and NP) on engine performance and emission characteristics, Analysis of Variance (ANOVA) was employed. The output variables considered were Brake Thermal Efficiency (BTE) and Oxides of Nitrogen (NOx) emissions. Each output variable was treated independently to isolate the individual and interaction effects of the predictors.

The dataset comprised 48 experimental observations, compiled into a Microsoft Excel file with five columns representing the three independent variables (IT, Load, NP) and two dependent variables (NOx, BTE). Prior to analysis, the data were examined for completeness, consistency, and outlier behavior.

The statistical analysis was conducted using Python (v3.10), executed within the Google Colaboratory environment. The primary statistical libraries utilized were pandas for data manipulation and import/export operations; statsmodels for performing ANOVA; and scipy and openpyxl for statistical computation and Excel file handling, respectively.

Each dependent variable was subjected to a three-way factorial ANOVA, considering the main effects and interaction effects of the independent variables. The significance of each factor and interaction was evaluated using the F-statistic, with corresponding p-values computed. A significance level of 0.05 was employed to determine statistical relevance. All

results, including the F-values, degrees of freedom, and *p*-values, were programmatically exported to an Excel workbook to facilitate reporting and reproducibility.

2.3. ANN Modeling

The ANN framework was implemented in MATLAB R2023b using the Levenberg–Marquardt (L–M) training algorithm, which is known for its superior convergence properties, especially in nonlinear function approximation problems.

The dataset comprised experimentally obtained input-output pairs corresponding to varying levels of three independent variables: IT, Load, and NP. Prior to modeling, all variables were normalized within the range of 0 to 1 to ensure numerical stability and uniform learning behavior across the network.

A feedforward backpropagation neural network architecture was constructed for each of the two target variables (BTE and NOx), with the following specifications:

- Input layer: 3 neurons (corresponding to IT, Load, and NP).
- Hidden layers: 1 hidden layer comprising 5 neurons with tangent sigmoid activation functions.
- Output layer: 1 neuron with a linear activation function, tailored for continuous regression output.

The Levenberg–Marquardt algorithm was chosen as the training function (trainlm in MATLAB) due to its hybrid optimization approach that combines the advantages of the gradient descent and Gauss–Newton methods, enabling rapid and accurate minimization of mean squared error (MSE) for nonlinear regression. The data were randomly partitioned into training (70%), validation (15%), and testing (15%) subsets. The network was trained iteratively until convergence criteria were met, typically defined by either a plateau in validation performance or a maximum of 1000 epochs. The coefficient of determination (R^2) was used to evaluate the model's predictive accuracy and generalization capability. Figure 2 shows the neural network architecture for the curve fitting of NOx and BTE with the input variables. The output equation is then obtained as shown in Equation (1).

$$y = W^o \cdot tansig\left(W^h \cdot x + b^h\right) + b^o \tag{1}$$

In matrix form, Equation (1) can be further represented as

$$z^h = W^h \cdot x + b^h \tag{2}$$

$$a^h = tansig\left(z^h\right) = \frac{2}{1 + e^{-2z^h}} - 1 \tag{3}$$

$$y = W^o \cdot a^h + b^o \tag{4}$$

where

$x = [x_1, x_2, x_3]^T$ is the input vector comprising injection timing, load, and nanoparticle size.
W^h and b^h are the weight matrix and bias vector of the hidden layer.
tansig is the hyperbolic tangent sigmoid function, which maps each neuron's input to the range $(-1, 1)$ and introduces nonlinearity to capture complex relationships.
W^o and b^o are the weight matrix and bias vector of the output layer.
$y = [y_1, y_2]^T$ is the output vector representing NOx and BTE.

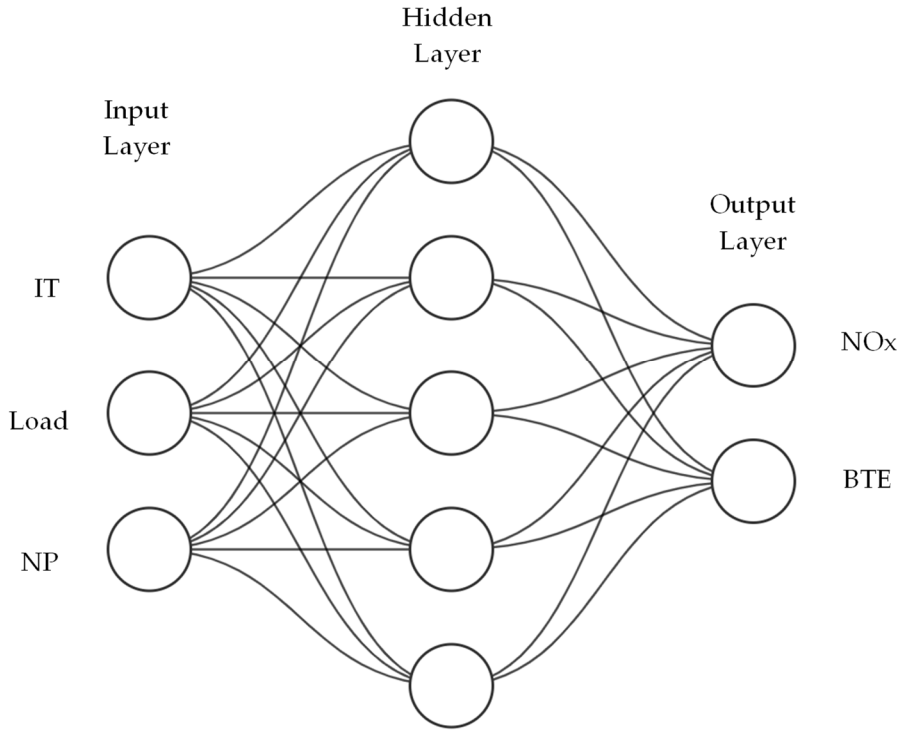

Figure 2. Neural network architecture for the curve fitting of NOx and BTE with the input variables (IT, Load, and NP).

Equations (2) and (3) correspond to hidden layer input and output matrices while Equation (4) is the final output layer response of NOx and BTE. The inputs of Load, IT, and NP were varied as (0, 100), (24, 30), and (0, 80), respectively.

The final ANN models exhibited high correlation with experimental data ($R^2 > 0.99$ for both responses), confirming their adequacy for use in downstream optimization. These trained models were subsequently exported and integrated into the Particle Swarm Optimization (PSO) framework as objective functions to derive the optimal operating conditions.

2.4. Response Surface Plots

To investigate the influence of engine operating parameters on the predicted outputs, two-dimensional contour plots were developed using a feedforward artificial neural network (ANN) model. The ANN architecture consisted of an input layer with three neurons corresponding to injection timing (IT), engine load (Load), and nanoparticle (NP) size. A single hidden layer with five neurons using a hyperbolic tangent sigmoid (tansig) activation function was used, and an output layer with two neurons representing nitrogen oxide (NOx, in ppm) and brake thermal efficiency (BTE, in %). The network was initially designed, trained, and validated in MATLAB R2023b using the Neural Network Toolbox.

After training, the network's structure, including the input-to-hidden and hidden-to-output weight matrices, biases, and normalization parameters, were exported from MATLAB. For the generation of contour plots, the ANN model was re-constructed in Python using the extracted weights and biases. Prior to feeding inputs to the model, each input variable was normalized using an affine transformation derived from the original MATLAB configuration. This ensured consistency between the original trained network and the reconstructed version. To visualize the relationship between the input variables and the model outputs, a uniform meshgrid of 100 × 100 resolution was generated across the domains of IT (27°–30° crank angle) and NP (0–100 nm). At the same time, Load was held constant at four representative values: 25%, 50%, 75%, and 100%. Each meshgrid point was combined with the fixed Load value to form an input matrix, which was then passed

through the reconstructed ANN. The network's hidden layer computed the activations using the tansig function, and the output layer applied a linear transformation. The resulting normalized outputs were then de-normalized using the inverse affine transformation to obtain NOx and BTE values in physical units.

The outputs corresponding to each meshgrid were reshaped into two-dimensional arrays and visualized using filled contour plots (contourf) with 20 evenly spaced contour levels. For each Load, separate contour plots were generated for NOx and BTE to enable clear interpretation.

2.5. Optimization Modeling

To identify the optimal operating conditions that simultaneously enhance BTE and reduce NOx emissions, a multi-objective optimization framework was adopted using the Particle Swarm Optimization (PSO) technique. The surrogate models for both objective functions were derived independently via ANN modeling (Section 2.3) for each load setting, trained on experimental data covering IT (ranging from 24 to 30°) and NP size (ranging from 0 to 80 nm).

The ANN-based mathematical expressions derived from Equation (1) served as surrogate models within the PSO framework. This approach facilitates a continuous, differentiable, and vectorizable formulation suitable for numerical optimization. As both BTE and NOX are of competing nature, the optimization problem was structured as a bi-objective minimization-maximization task, where NOx is to be minimized and BTE maximized.

The PSO algorithm employed was implemented in MATLAB 2023b. A proprietary version of the PSO code, developed and maintained by the authors in previous works [21,22], was utilized for this study. The algorithm was configured with the following parameters:

- Swarm size: 200 (calculated as 30 n, where n = 3 represents the number of process parameters).
- Inertia weight (w): 0.5 (constant across iterations).
- Cognitive coefficient (c1): 2.0.
- Social coefficient (c2): 2.0.
- Maximum iterations: 100.

Initial exploratory runs revealed convergence of non-dominated solutions within approximately 30 generations; thus, the maximum number of iterations was extended to 100 to ensure exhaustive exploration of the search space and to avoid premature convergence to local optima.

The PSO was constrained by upper and lower bounds for each decision variable, following experimentally feasible limits defined for IT, Load, and NP. The algorithm was executed without penalty functions due to the hard-bound nature of these constraints, which inherently ensured physical viability of the solutions. The optimization model thus, contained IT (24–30°), Load (0–100%), and NP (0–80 nm) as the input variables. The ANN equations of BTE and NOx developed using Equation (1) are the output variables.

The final output of the optimization comprised a Pareto front, representing the trade-off surface between BTE and NOx. This front was visualized in two-dimensional objective space to enable interpretation of optimal compromises between thermal performance and emission mitigation. The resulting solution set offers a practical decision space for engine tuning under dual-performance criteria, and the methodology provides a scalable framework for future optimization tasks involving multi-variable, multi-response objectives.

3. Results and Discussion

3.1. Experimental Results

The experimental study was conducted for three IT (24°, 27°, and 30° crank angle), four load settings (25%, 50%, 75%, and 100% of full load), and using NP sizes of 10 nm, 30 nm, and 80 nm. Figure 3a–c shows the emissions of NOx for IT of 24°, 27°, and 30°. Figure 3d–f shows the BTE for IT of 24°, 27°, and 30°.

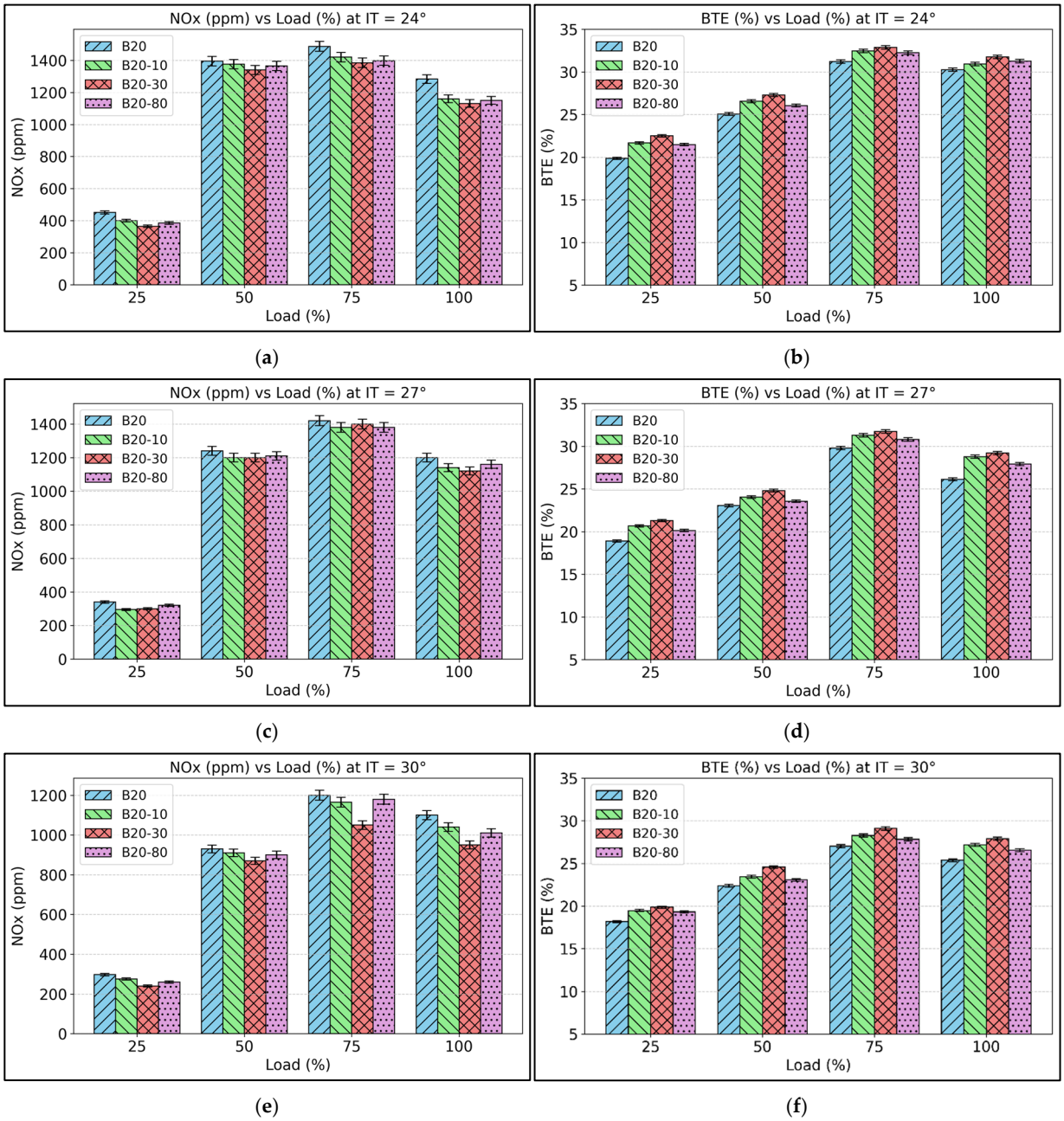

Figure 3. Emissions of NOx for IT of (**a**) 24°, (**c**) 27°, and (**e**) 30°; and brake thermal efficiencies (BTE) for (**b**) 24°, (**d**) 27°, and (**f**) 30°.

3.1.1. Effect of Engine Load on NOx and BTE

Engine load significantly influences both NOx formation and energy conversion efficiency. Across all tested injection timings and nanoparticle concentrations, increasing load from 25% to 75% leads to a marked increase in both NOx and BTE. However, this trend slightly reverses or saturates at 100% load. At low load (25%), NOx emissions are minimal

(average of 327 ppm), due to lower combustion temperatures and reduced oxygen demand. The combustion process is cooler and less vigorous, resulting in suppressed thermal NOx formation. As the load increases to 50% and 75%, the quantity of fuel injected increases proportionally, which enhances the in-cylinder pressure and temperature. Consequently, the formation of NOx through the Zeldovich mechanism is intensified due to elevated thermal energy and longer residence times at peak temperature. However, at full load (100%), although the fuel mass and pressure are at their maximum, the oxygen concentration becomes limiting. Locally rich mixtures and possible diffusion-controlled combustion regimes can reduce oxygen availability, marginally lowering NOx compared to 75% load. This points to a thermal–chemical limitation wherein excess fuel without proportional oxygen causes partial suppression of NOx, despite high combustion temperatures. These results are consistent with other findings in the literature [23,24].

The increase in BTE with load is largely thermodynamic, wherein higher loads increase the brake power output, thus improving the net efficiency. At 75% load, the peak BTE (30.4%) was observed, indicating optimal engine operation. At 100% load, a minor drop in BTE (28.6%) likely results from sub-optimal air-fuel mixing and elevated exhaust losses. Furthermore, under full-load conditions, late burning and heat rejection to cylinder walls are more significant, leading to reduced conversion of chemical energy into mechanical work.

3.1.2. Influence of CeO_2 Nanoparticles on Combustion and Emissions

Cerium oxide nanoparticles, known for their oxygen buffering and catalytic surface reactivity, impact the combustion process in multifaceted ways. Across all loads and injection timings, moderate NP sizes (up to 30 nm) improves BTE and reduces NOx, whereas higher sizes (80 nm) offer diminishing or even reversing benefits.

CeO_2 acts as a combustion promoter by releasing labile oxygen atoms at high temperatures, which then facilitates the complete oxidation of hydrocarbons and CO during combustion. The best BTE improvements were seen at 30 nm, particularly at medium to high loads. For instance, at 75% load and 30 nm NP, BTE peaked at 32.87%, higher than baseline diesel. This enhancement stems from improved micro-level fuel-air mixing, reduced ignition delay, and promotion of secondary oxidation reactions. While the initial NP sizes (10–30 nm) consistently reduced NOx, further increase to 80 nm showed a slight rebound in NOx levels. This nonlinearity may be due to excessive oxygen radicals from CeO_2 increasing combustion temperature locally. At 25% load and 30 nm, NOx dropped from 452 ppm (pure diesel) to 365 ppm, while BTE increased by nearly 3 percentage points. This indicates that NP sizes are most effective under light to medium load, where their catalytic role can compensate for slower combustion kinetics and insufficient mixing. Larger particles may also agglomerate more readily, decreasing fuel homogeneity and interfering with atomization quality, which can in turn reduce combustion efficiency and elevate NOx formation due to less uniform temperature distribution. Among the tested nanoparticle sizes, the 30 nm CeO_2 particles resulted in the most favorable balance between NOx reduction and BTE. While direct measurements of particle surface area or dispersion behavior were not conducted in this study, the observed trends are consistent with known effects in nanoparticle-supported combustion enhancement [25]. Smaller particles, such as 10 nm, are prone to agglomeration due to their high surface energy, which may reduce effective dispersion and catalytic activity. Conversely, larger particles like 80 nm offer fewer active sites due to lower surface area, limiting their contribution to combustion improvement. The 30 nm particles likely represent an optimal range where adequate surface area and stable dispersion enable efficient oxidation reactions and better combustion kinetics. Further research involving surface characterization and dispersion analysis would help to confirm

these mechanisms. It should, however, be noted that long-term studies assessing nanoparticle retention, potential agglomeration, and their fate in exhaust systems are essential for a holistic evaluation of the nanoparticle integration in the biofuel. Advanced exhaust treatment technologies, such as particulate filters or after-treatment systems, could be integrated to mitigate any residual particulate matter that might arise in practical applications.

3.1.3. Role of Injection Timing in NOx and Efficiency Trade-Off

Injection timing is a primary control parameter for combustion phasing. The test data span early (24° CA bTDC), mid (27°), and retarded (30°) injection timings. Advancing the injection timing (24° bTDC) increases ignition delay, allowing for more premixed combustion. This leads to a rapid and high-temperature pressure rise, significantly enhancing NOx formation. NOx emissions are highest at early injection (1487 ppm at 24°, 75% load, B20 neat). On the other hand, retarding the timing to 30° bTDC decreases the ignition delay, reducing the premixed burn phase and lowering the peak temperature. Consequently, NOx falls considerably. At 30°, average NOx dropped to 836 ppm, compared to 1093 ppm at 24°. This is physically consistent with the thermal sensitivity of NO formation, which is exponentially dependent on flame temperature.

However, delaying the injection also causes a drop in thermal efficiency. With late injection, combustion occurs closer to or even after TDC, reducing the expansion work and increasing wall heat losses. At 30°, BTE dropped to 24.34%, compared to 27.71% at 24°. The trade-off is evident, early injection favors power output but increases NOx; late injection controls NOX but reduces efficiency, that calls for an optimization.

The most insightful trends emerge from the combined effects of all three parameters. Considering the experimental trial having 24° IT, 75% Load, 30 nm NP, the NOx emissions were 1432 ppm at BTE of 32.87%**.** This combination leverages early injection for better efficiency and NP for improved combustion. However, it sacrifices NOx control due to the inherent thermal load from premixed combustion. However, at 30° IT, 25% Load, 30 nm NP, the NOx emissions dropped to 240 ppm with a BTE of 19.85%. Retarded timing and low load combine to suppress NOx drastically. NPs compensate slightly for efficiency loss but cannot fully overcome the combustion delay and energy inefficiency at low load. Figure 4 shows the response surface plots for NOx and BTE separately for 25%, 50%, 75%, and 100% of full load. These comparisons underscore that no single parameter alone governs combustion behavior. Instead, it is the interplay between load-dependent thermodynamics, injection-driven combustion phasing, and NP-catalyzed oxidation that determines engine response. Hence, to understand the most optimal levels of the inputs, the NOx and BTE were modeled using an ANN and optimization has been carried out using PSO.

3.2. ANOVA Results

The experimental data was statistically examined using Analysis of Variance (ANOVA), and the *p*-values derived from this analysis are summarized in Table 3. Injection timing was found to have a statistically significant effect on both NOx ($p = 0.017$) and BTE ($p = 8.58 \times 10^{-5}$), well below the accepted $\alpha = 0.05$ threshold. Advancing the injection timing tends to increase in-cylinder pressure and peak temperature due to longer ignition delay and increased premixed combustion. The observed significance implies that even small changes in timing can measurably alter both emissions and efficiency, underlining its importance in optimization strategies for modern CI engines. Load exerted the most dominant influence on both NOx ($p = 4.21 \times 10^{-8}$) and BTE ($p = 1.01 \times 10^{-13}$), with *p*-values several orders of magnitude lower than the significance threshold. As engine load increases, more fuel is injected per cycle to meet the power demand. This increases the amount of heat released and elevates the in-cylinder pressure and temperature. As a result, both BTE

and NOx emissions typically increase. The rise in BTE with load is physically attributed to better utilization of fuel energy due to higher combustion pressure and improved cylinder filling, while the increase in NOx stems from higher thermal gradients. The exceptionally low *p*-values reinforce that load is a first-order effect in engine performance and emission behavior. NP size significantly affected both NOx ($p = 0.0375$) and BTE ($p = 0.0452$). Cerium oxide nanoparticles are known oxygen buffers and combustion catalysts. They promote oxidation of soot precursors and facilitate more complete combustion. This can lead to enhanced thermal efficiency (observed here as a statistically significant improvement in BTE) and affects the emission characteristics. At low sizes, CeO_2 may enhance combustion and reduce NOx due to better oxidation, but at higher sizes, localized oxygen enrichment may raise flame temperatures, counteracting the NOx reduction. The statistical results capture this nuanced impact, which is often masked in simple trend analyses. None of the two-way interactions (IT × Load, IT × NP, Load × NP) were statistically significant for either NOX or BTE, with all *p*-values above 0.27 and most nearing 1. The absence of significant interaction effects implies that the individual contributions of IT, Load, and NP are largely independent in their influence on the response variables. In other words, the effect of changing injection timing is not significantly altered by the level of load or NP size, and vice versa. This simplifies the interpretation and modeling of engine behavior, suggesting an additive model structure rather than a highly coupled system. The ANOVA analysis supports a clear ranking framework for CI engine optimization. While load cannot always be arbitrarily adjusted, understanding its impact is crucial in load-following applications. IT offers a practical means to simultaneously target NOx and BTE, although a trade-off typically exists, necessitating multi-objective optimization. NP size provides a promising, chemically tunable route to enhance combustion performance, albeit with diminishing returns or conflicting effects at higher concentrations. Importantly, the lack of interaction effects simplifies the modeling and control strategies, enabling more robust calibration of engines across different operating regimes. Although the ANOVA results in Table 3 show significant main effects for injection timing, load, and nanoparticle size, the interaction terms are not statistically significant at 95% confidence level. However, the response surface plots in Figure 4 visually suggest interaction-like trends between the parameters. This apparent discrepancy arises because the ANOVA tests interaction effects based on predefined linear or polynomial relationships, whereas the ANN model used to generate the response surfaces captures complex nonlinear relationships that can produce interaction patterns even when formal interaction terms are not statistically significant. Therefore, the visual trends observed in Figure 4 are consistent with the nonlinear behavior learned by the model and do not contradict the ANOVA findings. This distinction is important in interpreting the results and reinforces the complementary roles of statistical analysis and machine learning-based modeling.

Table 3. ANOVA table for different input parameters and their interaction effects.

Variable	*p*-Value		Significance
	NOx	BTE	
IT	0.017253	8.58×10^{-5}	Significant
Load	4.21×10^{-8}	1.01×10^{-13}	Significant
NP	0.0375	0.0452	Significant
IT × Load	0.896	0.275	Not Significant
IT × NP	0.928	0.907	Not Significant
Load × NP	0.915	0.999	Not Significant

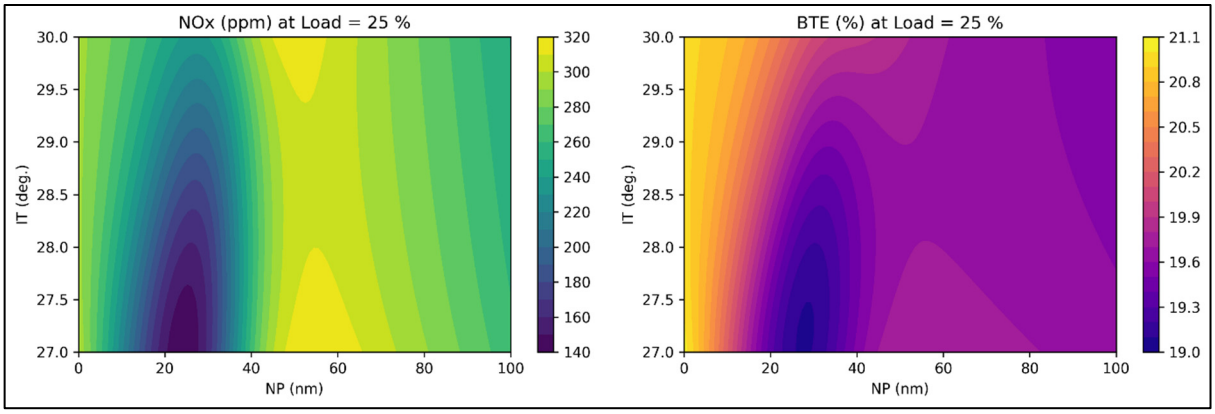

(**a**)

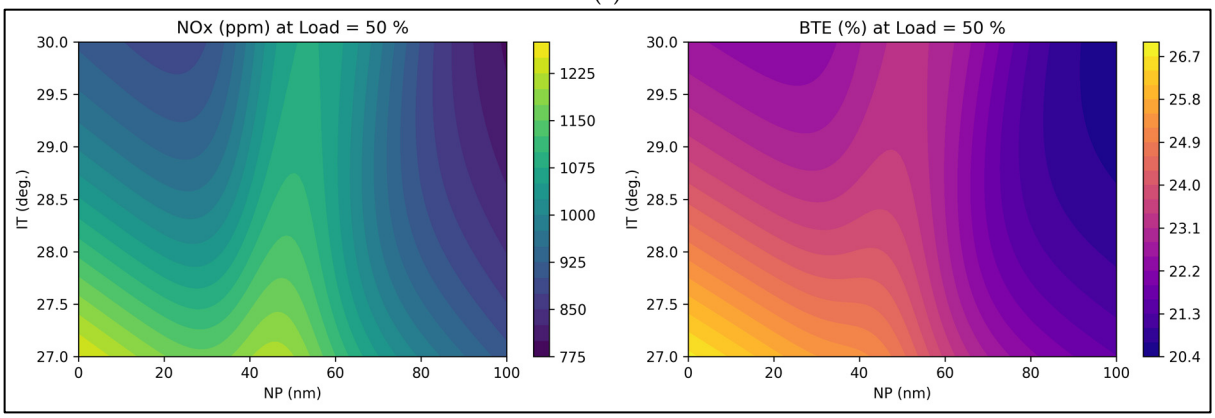

(**b**)

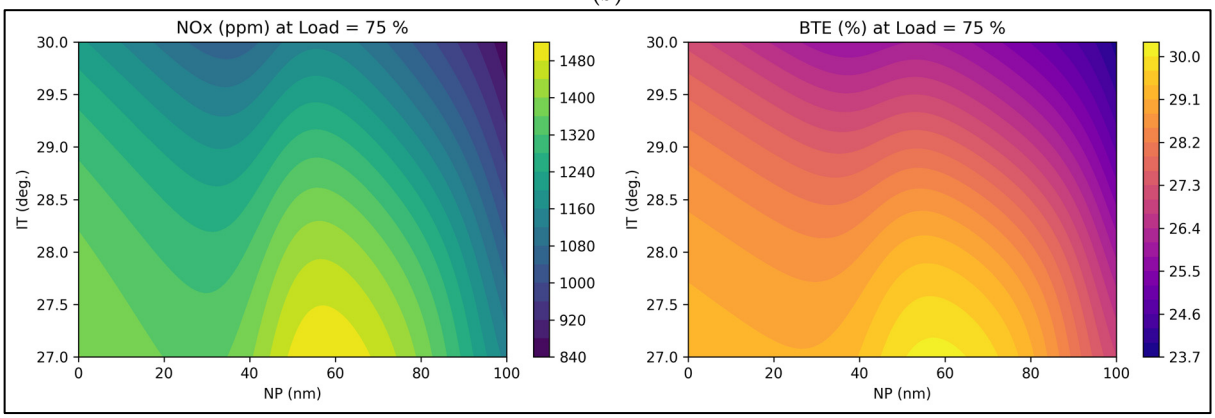

(**c**)

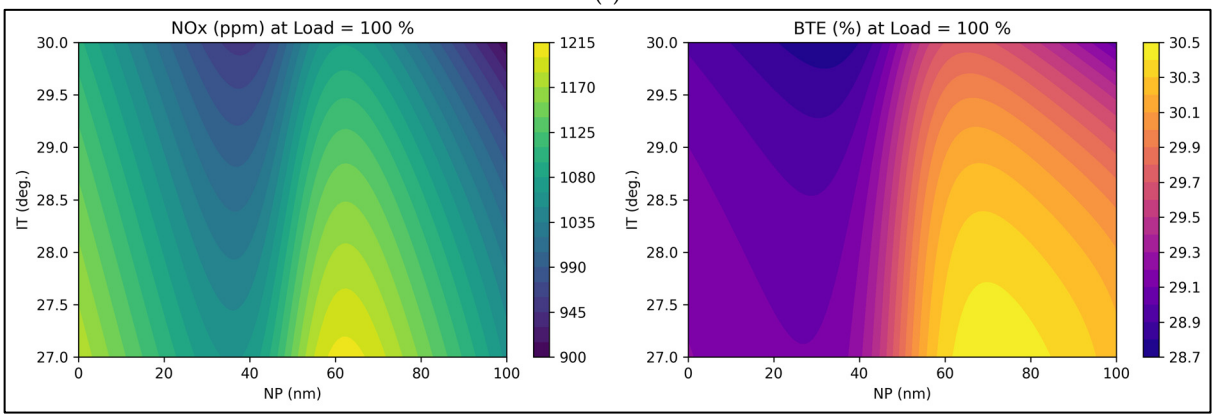

(**d**)

Figure 4. Response surface plots for NOx and BTE obtained using ANN model for load variation at (**a**) 25%, (**b**) 50%, (**c**) 75%, and (**d**) 100%.

3.3. Optimization Using ANN-PSO

The ANN models for BTE and NOx prediction achieved coefficients of determination (R^2), exceeding 0.99 for training, validation, and testing, confirming the models' robustness. The corresponding weight and bias coefficients are provided in Table S1 (Supplementary Material). These ANN equations were subsequently integrated into the PSO framework, wherein the ANN outputs served as objective functions. The optimization yielded a Pareto front representing the trade-off between BTE and NOx reduction. The non-dominated solutions define the feasible region for engine calibration, enabling selection of optimal operating conditions under dual-performance criteria. Recognizing that engine load exerts a dominant influence on both combustion kinetics and emissions profile, the optimization process was segregated into four distinct load points (25%, 50%, 75%, and 100% of full load). This load-specific optimization strategy not only ensures practical relevance but also captures the nonlinear influence of load on the response surface. The optimization results and their corresponding experimental validations are summarized in Table 4. Figure 5 shows the Pareto front of the optimized NOx against the corresponding optimized BTE for each of the four distinct loads. For each load condition, the PSO algorithm converged to a unique combination of IT and NP that offered the best trade-off between NOx and BTE.

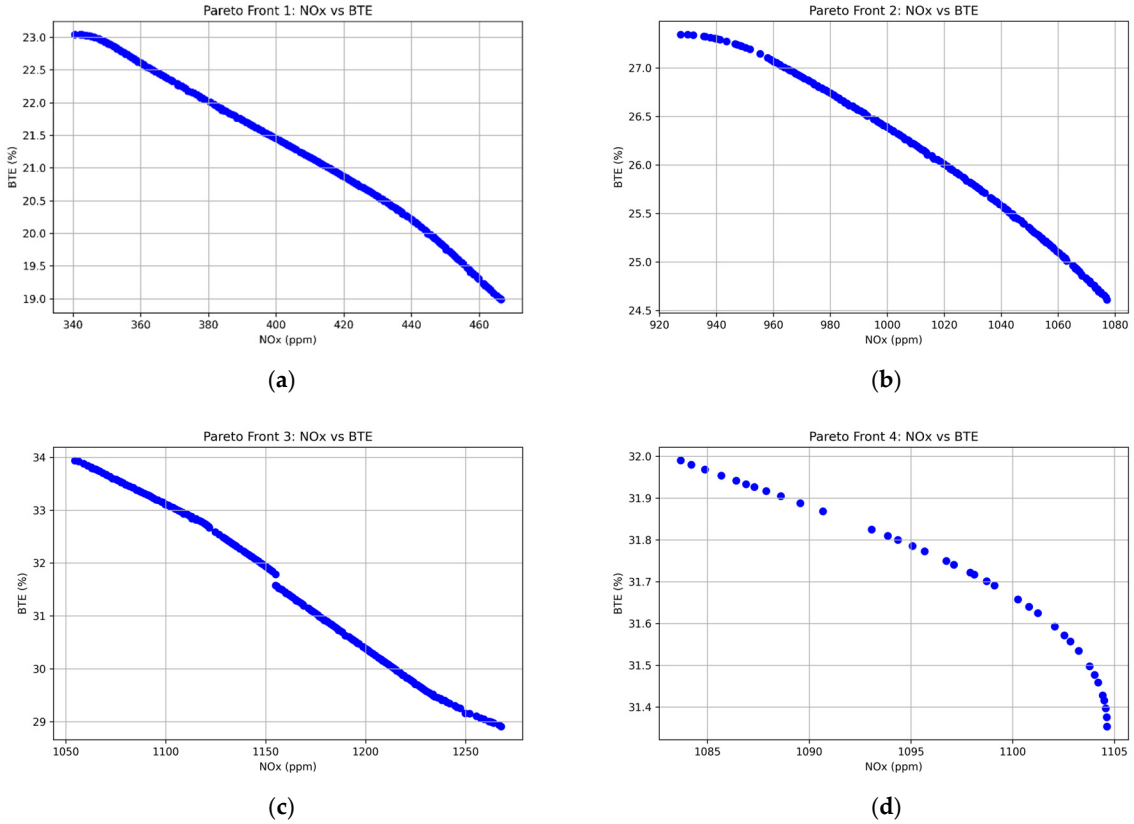

Figure 5. Plot of Pareto front of the optimized objective functions (NOx and BTE) after executing PSO for engine loads of (**a**) 25%, (**b**) 50%, (**c**) 75%, and (**d**) 100%.

At low load (25%), the optimized injection timing of 26.66 and NP size of 33 nm yielded a PSO-predicted NOx emission of 407 ppm and a BTE of 21.17%. Experimentally, the NOx value was even lower at 305 ppm, with a comparable BTE of 21.1%. This close agreement validates the ANN-PSO model's accuracy at low thermal loads. The relatively advanced injection timing favors better combustion initiation due to the lower cylinder pressure and temperature at light loads. Simultaneously, CeO_2 nanoparticles likely act as

combustion catalysts and oxygen donors, improving oxidation of unburnt hydrocarbons without substantially increasing NOx formation due to lower peak flame temperatures.

At 50% load, the model predicts an optimum timing of 28.40° and an elevated NP size of 45 nm. This configuration yields a PSO NOx value of 1021 ppm and a BTE of 25.99%, against an experimental NOx of 1108 ppm and BTE of 24.6%. The modest underprediction of NOx by the PSO model may stem from localized hot spots or insufficient mixing at this intermediate load. However, the rise in BTE reflects improved energy conversion due to enhanced ignition delay and better premixing.

Table 4. Validation of the results obtained from the ANN-PSO model with the experimental data.

Load	PSO				Experimental			
	IT (°)	**NP (nm)**	**NOx (ppm)**	**BTE (%)**	**IT (°)**	**NP (nm)**	**NOx (ppm)**	**BTE (%)**
25%	26.66	33.07	407	21.17	27.00	30.00	305 ± 6	21.11 ± 0.14
50%	28.40	44.85	1021	25.99	27.00	50.00	1108 ± 23	24.62 ± 0.16
75%	27.95	35.78	1160	31.49	27.00	30.00	1272 ± 27	32.13 ± 0.21
100%	30.00	21.92	1096	31.71	30.00	20.00	996 ± 21	28.58 ± 0.19

In the 75% load regime, optimization suggests an injection timing of 27.95° and 36 nm NP, resulting in 1160 ppm NOx and a BTE of 31.49%. Experimental values closely mirror these with 1272 ppm NOx and a slightly higher BTE of 32.1%. Here, the combustion dynamics are governed by a more favorable pressure-temperature regime, wherein the NP's oxygen-buffering and thermal conductivity-enhancing characteristics promote flame stability. The marginal underestimation of BTE by the model may indicate a need for finer granularity in the surrogate model or slight experimental deviations in fuel-air stratification.

At full load (100%), the optimal configuration shifts to a delayed injection timing of 30° and reduced NP size (22 nm), resulting in 1096 ppm NOx and 31.71% BTE via PSO. The experimental NOx value of 996 ppm is notably lower, whereas the experimental BTE (28.58%) trails the predicted value. The larger error in BTE here is possibly due to heat losses at high loads that the ANN-based surrogate model could not fully capture. The relatively retarded injection timing at high load is thermodynamically justified as it mitigates NOx formation by limiting the peak temperature, while the reduced NP size prevents excess catalytic surface area that could unintentionally favor NOx chemistry under these aggressive conditions.

The trend across load points describes the nonlinear and coupled influence of injection timing and NP size. Injection timing increases with load, shifting from 26.66° at 25% load to 30° at full load. This advancement reflects the requirement for longer ignition delays and better charge preparation under higher pressure conditions. NP size shows a parabolic trend, peaking at 50% load. At lower loads, CeO_2 improves combustion without triggering NOx penalties, while at full load, excessive nanoparticles may aggravate NOx due to elevated in-cylinder temperatures and secondary oxidation pathways. The trade-off between BTE and NOx becomes more pronounced with load. At low loads, combustion inefficiencies dominate; at high loads, the thermal NOx mechanism seems to be the controlling factor. The PSO framework effectively navigates this trade-off.

The PSO results were experimentally validated using engine trials at the predicted optimal operating conditions. The relative error between model-predicted and experimental NOx values for 25%, 50%, 75%, and 100% loads were, respectively, 25.1%, 8.5%, 9.7%, and 9.1%, with an overall mean of 8.8%. Similarly, the relative error concerning BTE for the same four loads was, respectively, 0.3%, 5.3%, 2.0%, and 9.9% with an overall mean of 4.4%. The

application of the ANN-PSO optimization framework yielded noticeable improvements in engine performance and emissions across different load conditions. At 25% load, the average BTE across all tested nanoparticle sizes and injection timings was 20.23%, which improved to 21.1% after optimization. Similarly, at 50% load, the average BTE of 24.49% increased to 24.62%; at 75% load, a significant improvement from 30.38% to 32.13% was observed; and at 100% load, the BTE remained stable with a slight adjustment from 28.59% to 28.58%. In terms of NOx emissions, substantial reductions were achieved: at 25% load, average emissions of 327 ppm decreased to 305 ppm; at 50% load, 1161 ppm reduced to 1108 ppm; at 75% load, 1322 ppm decreased to 1272 ppm; and at 100% load, 1120 ppm dropped to 996 ppm. These results demonstrate the effectiveness of the integrated ANN-PSO approach in identifying optimal combinations of injection timing and nanoparticle size, particularly at moderate loads where improvements in combustion efficiency and emission control were most pronounced. These values are within acceptable bounds for optimization using the hybrid ANN-PSO technique, especially considering real-world engine variability. The relatively high reliability of the model underlines the robustness of the ANN-PSO framework. The results also suggest that load-specific optimization strategies are superior to global models when dealing with systems exhibiting strong nonlinear behavior and cross-parameter interactions.

4. Conclusions

This study investigated the combined influence of injection timing and cerium oxide (CeO_2) nanoparticle size on NOx emissions and brake thermal efficiency (BTE) in a CI engine under varying loads. The experimental data showed that both injection timing and nanoparticle addition significantly influenced engine performance. CeO_2 nanoparticles improved BTE across all loads due to their oxygen buffering and catalytic activity, but their effect on NOx emissions was load-dependent. At higher loads, NOx increased slightly due to elevated combustion temperatures, despite the presence of nanoparticles.

ANOVA analysis confirmed the statistical significance of the input parameters. Load was the most dominant factor influencing both NOx ($p = 4.21 \times 10^{-8}$) and BTE ($p = 1.01 \times 10^{-13}$). Injection timing (IT) also had a strong effect ($p < 0.05$), affirming its role in combustion phasing and thermal efficiency. Nanoparticle size (NP) showed moderate but significant influence on both NOx ($p = 0.0375$) and BTE ($p = 0.0452$). Interaction terms between variables, however, were statistically insignificant, indicating minimal interdependence.

To identify optimal conditions, multi-objective particle swarm optimization (PSO) was performed separately for each load level. The goal was to minimize NOx while maximizing BTE. At all loads, the PSO algorithm successfully provided injection timing and nanoparticle concentration values close to the experimentally validated optimum. The differences between PSO-predicted and actual experimental outcomes remained within acceptable limits, demonstrating the validity of the surrogate model used.

Overall, this integrated study demonstrates that injection timing and nanoparticle dosage must be fine-tuned based on engine load. The proposed ANN–PSO framework is a powerful tool for identifying these optimal conditions. This approach can serve as a basis for developing real-time engine control strategies for improved efficiency and reduced emissions in future diesel engine applications. Future research will include a detailed life cycle assessment to quantify the environmental and economic impacts associated with the production and use of cerium oxide nanoparticles in biodiesel blends. This will help to better understand the net sustainability benefits and trade-offs, ensuring alignment with global climate goals and energy accessibility objectives.

Supplementary Materials: The following supporting information can be downloaded at https://www.mdpi.com/article/10.3390/su17209004/s1: Table S1: Consolidated table showing the weights and biases of ANN modeling (for NOx and BTE).

Author Contributions: Conceptualization, P.D.; Data Curation, S.M.; Formal Analysis, S.M. and K.A.; Funding Acquisition, A.N. and J.P.; Methodology, S.M., P.D. and R.K.G.; Software, S.M. and K.A.; Supervision, P.D.; Visualization, S.M.; Writing—original draft, S.M., K.A. and P.D.; Writing—Review and Editing, R.K.G., A.N. and J.P. All authors have read and agreed to the published version of the manuscript.

Funding: The authors extend their acknowledgement to the financial support of the European Union under the REFRESH-Research Excellence For REgion Sustainability and High-tech Industries, project number CZ.10.03.01/00/22_003/0000048, via the Operational Programme Just Transition.

Institutional Review Board Statement: Not applicable.

Informed Consent Statement: Not applicable.

Data Availability Statement: The raw data supporting the conclusions of this article will be made available by the authors on request.

Conflicts of Interest: The authors declare no conflicts of interest.

References

1. Luo, H.; Liu, L.; Nishida, K.; Zhou, W. Development and Utilization on Green Energy in Marine Powertrain: Challenges and Opportunities. *Green Energy Resour.* **2024**, *2*, 100076. [CrossRef]
2. International Energy Agency. *Global Energy Review 2025*; International Energy Agency: Paris, France, 2025.
3. United Nations. *The Sustainable Development Goals Report 2024*; United Nations: New York, NY, USA, 2024.
4. Suhara, A.; Karyadi; Herawan, S.G.; Tirta, A.; Idris, M.; Roslan, M.F.; Putra, N.R.; Hananto, A.L.; Veza, I. Biodiesel Sustainability: Review of Progress and Challenges of Biodiesel as Sustainable Biofuel. *Clean Technol.* **2024**, *6*, 886–906. [CrossRef]
5. Kumar, M.; Bhowmik, S.; Paul, A. Effect of Pilot Fuel Injection Pressure and Injection Timing on Combustion, Performance and Emission of Hydrogen-Biodiesel Dual Fuel Engine. *Int. J. Hydrogen Energy* **2022**, *47*, 29554–29567. [CrossRef]
6. Saravanan, B.; Asokan, M.A. Impact of Fuel Injection Parameters and Hydrogen Enrichment on CI Engine Characteristics Fueeled with Ceiba Pentandra Biodiesel. *Energy Sources Part A Recovery Util. Environ. Eff.* **2024**, *46*, 3734–3747. [CrossRef]
7. Asokan, M.A.; Prabu, S.S.; Musthafa, B.; Saravanan, B.; Sujai, S.; Pote, R.T.; Chavan, N.P.; Bhor, D.S. Effect of Antioxidants on CI Engine Characteristics of Safflower Biodiesel with Varying Fuel Injection Pressures. *Case Stud. Therm. Eng.* **2024**, *60*, 104658. [CrossRef]
8. Zhai, C.; Zhang, J.; Li, K.; Dong, P.; Jin, Y.; Chang, F.; Luo, H. Comparative Analysis and Normalization of Single-Hole vs. Multi-Hole Spray Characteristics: 1st Report on Spray Characteristic Comparison. *Green Energy Resour.* **2025**, *3*, 100120. [CrossRef]
9. Ali Ijaz Malik, M.; Kalam, M.A.; Mujtaba Abbas, M.; Susan Silitonga, A.; Ikram, A. Recent Advancements, Applications, and Technical Challenges in Fuel Additives-Assisted Engine Operations. *Energy Convers. Manag.* **2024**, *313*, 118643. [CrossRef]
10. Truong, T.T.; Nguyen, X.P.; Pham, V.V.; Le, V.V.; Le, A.T.; Bui, V.T. Effect of Alcohol Additives on Diesel Engine Performance: A Review. *Energy Sources Part A Recovery Util. Environ. Eff.* **2025**, *47*, 2011490. [CrossRef]
11. Yamini, K.; Kishore, P.S.; Dhana Raju, V. Effect of Diethyl Ether and Isobutanol as Fuel Additives on the Diesel Engine Attributes Fueled with Subabul Seed Biodiesel. *J. Therm. Eng.* **2025**, *11*, 215–225. [CrossRef]
12. Ramalingam, S.; Sampath, S.; Krishnamoorthi, T.; Saravanamuthu, M.; Dillikannan, D. Comprehensive Assessment of Energy, Exergy, and Environmental Impacts of Lemongrass Oil-Diesel Blend with Dimethyl and Diethyl Ethers in Agricultural Diesel Engines. *Chem. Eng. Process.—Process Intensif.* **2025**, *209*, 110187. [CrossRef]
13. Singh, M.; Saini, P.; Srivastava, D.; Mishra, S.; Ahmad, S.N. Effect of N-Pentanol with Novel Water Hyacinth Biodiesel-Diesel Ternary Blends on Diesel Engine Performance and Emission Characteristics. *Vietnam J. Chem.* **2024**, *62*, 780–791. [CrossRef]
14. Rangabashiam, D.; Munuswamy, D.B.; Duraiswamy Balasubramanian, S.; Christopher, D. Performance, Emission, and Combustion Analysis on Diesel Engine Fueled with Blends of Neem Biodiesel/Diesel/ Additives. *Energy Sources Part A Recovery Util. Environ. Eff.* **2024**, *46*, 8059–8069. [CrossRef]
15. Hamzah, A.H.; Akroot, A.; Abdul Wahhab, H.A.; Ghazal, R.M.; Alhamd, A.E.J.; Bdaiwi, M. Effects of Nano-Additives in Developing Alternative Fuel Strategy for CI Engines: A Critical Review with a Focus on the Performance and Emission Characteristics. *Results Eng.* **2024**, *22*, 102248. [CrossRef]

16. Zheng, F.; Cho, H.M. The Comprehensive Effects of Nano Additives on Biodiesel Engines—A Review. *Energies* **2024**, *17*, 4126. [CrossRef]
17. Modi, V.; Rampure, P.B.; Babbar, A.; Kumar, R.; Nagaral, M.; Bhowmik, A.; Pandey, S.; Hasnain, S.M.M.; Ali, M.M.; Bashir, M.N. Nanoparticle-Enhanced Biodiesel Blends: A Comprehensive Review on Improving Engine Performance and Emissions. *Mater. Sci. Energy Technol.* **2024**, *7*, 257–273. [CrossRef]
18. Gad, M.S.; Hashish, H.M.A.; Hussein, A.K.; Ben Hamida, M.B.; Abdulkader, R.; Nasef, M.H. Effect of Different Configurations of Hybrid Nano Additives Blended with Biodiesel on CI Engine Performance and Emissions. *Sci. Rep.* **2024**, *14*, 19528. [CrossRef]
19. Bhan, S.; Gautam, R.; Singh, P. Analyzing the Impact of Adding Aluminum Oxide and Cerium Oxide Nanoparticles to Waste Cooking Biodiesel on Engine Performance, Combustion and Emissions Characteristics. *Pet Sci. Technol.* **2024**, *42*, 706–734. [CrossRef]
20. Hoang, A.T. Combustion behavior, performance and emission characteristics of diesel engine fuelled with biodiesel containing cerium oxide nanoparticles: A review. *Fuel Proc. Technol.* **2021**, *218*, 106840. [CrossRef]
21. Mohan, S.; Dinesha, P.; Campana, P.E. ANN-PSO Aided Selection of Hydrocarbons as Working Fluid for Low-Temperature Organic Rankine Cycle and Thermodynamic Evaluation of Optimal Working Fluid. *Energy* **2022**, *259*, 124968. [CrossRef]
22. Barboza, A.B.V.; Mohan, S.; Dinesha, P. On Reducing the Emissions of CO, HC, and NOx from Gasoline Blended with Hydrogen Peroxide and Ethanol: Optimization Study Aided with ANN-PSO. *Environ. Pollut.* **2022**, *310*, 119866. [CrossRef]
23. Yu, Y.; Xu, L.; Niu, Y. Synergistic reduction of PM and NOx in different preheating co-firing modes of coal and biomass. *J. Energy Inst.* **2025**, *121*, 102151. [CrossRef]
24. Gaur, R.K.; Goyal, R. Performance, Emission, Combustion and Economics Analysis of CI Engine Fueled with Mixed Oil Biodiesel Blends from Waste Cooking Oil and Pongamia Oil. *Discov. Appl. Sci.* **2025**, *7*, 609. [CrossRef]
25. Alshora, D.H.; Ibrahim, M.A.; Alanazi, F.K. Chapter 6—Nanotechnology from Particle Size Reduction to Enhancing Aqueous Solubility. In *Surface Chemistry of Nanobiomaterials*; Grumezescu, A.M., Ed.; William Andrew Publishing: Norwich, NY, USA, 2016; pp. 163–191. ISBN 978-0-323-42861-3.